Brazilian Journal of Medical and Biological Research (2014) 47(10): 850-857, http://dx.doi.org/10.1590/1414-431X20143679
ISSN 1414-431X

Dynamic expression of *desmin*, α-*SMA* and *TGF-β1* during hepatic fibrogenesis induced by selective bile duct ligation in young rats

J.O. Gonçalves, A.C.A. Tannuri, M.C.M. Coelho, I. Bendit and U. Tannuri

Laboratório de Pesquisa em Cirurgia Pediátrica (LIM-30), Faculdade de Medicina, Universidade de São Paulo, São Paulo, SP, Brasil

Abstract

We previously described a selective bile duct ligation model to elucidate the process of hepatic fibrogenesis in children with biliary atresia or intrahepatic biliary stenosis. Using this model, we identified changes in the expression of *alpha smooth muscle actin* (α-*SMA*) both in the obstructed parenchyma and in the hepatic parenchyma adjacent to the obstruction. However, the expression profiles of *desmin* and *TGF-β1*, molecules known to be involved in hepatic fibrogenesis, were unchanged when analyzed by semiquantitative polymerase chain reaction (RT-PCR). Thus, the molecular mechanisms involved in the modulation of liver fibrosis in this experimental model are not fully understood. This study aimed to evaluate the molecular changes in an experimental model of selective bile duct ligation and to compare the gene expression changes observed in RT-PCR and in real-time quantitative PCR (qRT-PCR). Twenty-eight Wistar rats of both sexes and weaning age (21-23 days old) were used. The rats were separated into groups that were assessed 7 or 60 days after selective biliary duct ligation. The expression of *desmin*, α-*SMA* and *TGF-β1* was examined in tissue from hepatic parenchyma with biliary obstruction (BO) and in hepatic parenchyma without biliary obstruction (WBO), using RT-PCR and qRT-PCR. The results obtained in this study using these two methods were significantly different. The BO parenchyma had a more severe fibrogenic reaction, with increased α-*SMA* and *TGF-β1* expression after 7 days. The WBO parenchyma presented a later, fibrotic response, with increased *desmin* expression 7 days after surgery and increased α-*SMA* 60 days after surgery. The qRT-PCR technique was more sensitive to expression changes than the semiquantitative method.

Key words: *Alpha smooth muscle actin*; *Desmin*; Hepatic fibrogenesis; Selective bile duct ligation; RT-PCR; *TGF-β1*

Introduction

The mechanisms leading to increased collagen production and liver parenchyma fibrosis are poorly understood (1). These phenomena are commonly observed in children with biliary atresia, in whom the evolution to biliary cirrhosis and hepatic failure creates a need for liver transplantation in the majority of patients, even after a successful Kasai portoenterostomy (2).

Similarly, pediatric liver transplantation presents with biliary complications in 20 to 30% of cases in the postoperative period (3). Intra- or extra-hepatic stenosis of the bile ducts is frequent and may lead to secondary biliary cirrhosis and the need for retransplantation (3,4). It is unknown whether biliary stenosis involving isolated segments or lobes can affect the adjacent unobstructed lobes by paracrine or endocrine signaling, leading to fibrosis in the neighboring parenchyma (5-7). In order to investigate this possibility, we developed a selective bile duct ligation model in weaning rats. In that model, we observed that biliary proliferation and portal fibrosis occurred in both the cholestatic and the unobstructed lobes of the liver in response to biliary obstruction (1).

During liver fibrogenesis, hepatic stellate cells or Ito cells are activated and differentiate into myofibroblasts (8). In rats, the activation and proliferation of stellate cells correlates with a high expression of *desmin* (9), while *alpha smooth muscle actin* (α-*SMA*) is considered a myofibroblast marker because it is expressed after the differentiation of these cells (8). Desmin and α-SMA are structural intermediate filament proteins present in the cytoskeleton of smooth muscle cells and other cell types (8,9). These cells are responsible for the increased type I collagen synthesis observed in liver fibrogenesis (10). Another important profibrogenic cytokine involved in this process is transforming growth factor beta (TGF-β1)

Correspondence: U. Tannuri, Faculdade de Medicina, Universidade de São Paulo, Avenida Dr. Arnaldo 455, 4º andar, Sala 4109, 01246-903 São Paulo, SP, Brasil. Fax: +55-11-3255-6285. E-mail: uenist@usp.br

Received November 6, 2013. Accepted April 29, 2014. First published online August 15, 2014.

(8-10), which transcriptionally regulates type I collagen expression in stellate cells (11).

Molecular analyses performed by conventional semi-quantitative polymerase chain reaction (RT-PCR) in our rat model revealed increases in only α-*SMA* gene expression, in both obstructed and unobstructed liver parenchyma; the expression of *desmin* and *TGF-β1* genes was unchanged (1).

On the other hand, real-time quantitative polymerase chain reaction (qRT-PCR) has previously been described as a more precise and sensitive method for molecular analysis than conventional RT-PCR. Therefore, the objectives of the present study were to evaluate the molecular changes in an experimental model of selective bile duct ligation and to compare the gene expression changes observed with the RT-PCR and qRT-PCR methods.

Material and Methods

Animals

Twenty-eight Wistar rats of weaning age (21-23 days of age and weighing 30-50 g) were used. All animals received care according to the criteria outlined in the Guide for the Care and Use of Laboratory Animals prepared by the National Academy of Sciences (12). The protocol for this study was approved by the animal Ethics Committee of Faculdade de Medicina, Universidade de São Paulo, São Paulo, Brazil.

The weaned rats were maintained on a standard laboratory diet and tap water *ad libitum* throughout the experiment.

Surgical procedures

The surgical procedures were performed under sterile conditions using isofurane anesthesia. Animals were submitted to selective ligation of the biliary ducts as previously described (1). The bile ducts of the median, left lateral, and caudate liver lobes were ligated, and biliary drainage of the right lateral lobe was left intact (Figure 1).

Rats were euthanized 7 or 60 days after the operation (7 animals per group) under isofurane anesthesia. A midline abdominal and thoracic incision was performed to harvest the liver lobes. The median and left lateral lobes with biliary obstruction (BO) and the right lateral lobe without biliary obstruction (WBO) were harvested separately. Liver tissue from age-matched rats (28 and 81 days of age, 7 per group) not subjected to ligation surgery was used as a control.

Liver tissues were snap frozen at –170°C in liquid nitrogen for subsequent molecular analyses. The expression of *desmin*, α-*SMA*, and *TGF-β1* was assessed using both RT-PCR and qRT-PCR.

Total RNA isolation and reverse transcription

Total RNA was isolated from frozen liver samples using TRIZOL (Invitrogen, USA) according to the manufacturer's protocol. Total RNA was quantified with spectrophotometry using a Biophotometer (Eppendorf AG, Germany) at an absorbance of 260 nm, and the purity was assessed using the 260/280 nm absorbance ratio. This value ranged from 1.8 to 2 for all samples. The integrity of the isolated RNA samples was determined by agarose gel electrophoresis and ethidium bromide staining of the 18S and 28S ribosomal RNA bands.

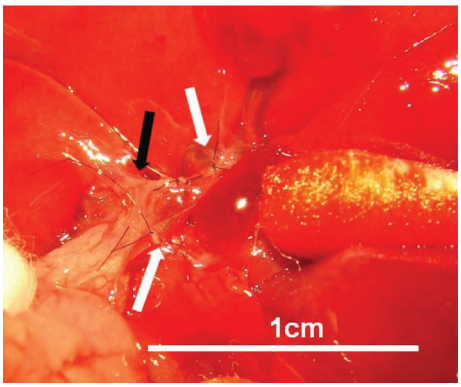

Figure 1. Photograph showing the ligation and section of the median, left lateral, and caudate liver lobe ducts. Note that the bile duct of the right lateral lobe was left intact (black arrow).

Complementary DNA (cDNA) was prepared from 2 μg total RNA by reverse transcription using 200 U of SuperScript III RNase H-RT (Invitrogen) and oligo (dT) primers. The resulting cDNA was stored at –20°C.

Primers specific for *desmin*, α-*SMA*, and *TGF-β1* were designed based on the rat messenger RNA sequences from the GenBank database using the Primer3 software (http://www.bioinformatics.nl/cgi-bin/primer3plus/primer3plus.cgi/). As an internal reference, primers for *cyclophilin* and *hypoxanthine phosphoribosyl transferase* were used. The primer sequences and size of the amplified products are listed in Table 1.

RT-PCR

Semiquantitative RT-PCR was performed in a total volume of 25 μL containing 100 ng cDNA, 20 pmol of each primer, 200 μmol dNTPs, 1.5 mM $MgCl_2$, 2.5 μL of 10× PCR buffer (Invitrogen), and 2 units Taq polymerase (Invitrogen). The reaction was carried out in a PTC 200 thermocycler (MJ Research, USA), accompanied by a control reaction to identify contamination. The thermal cycler reaction conditions were as follows: initial denaturation for 5 min at 94°C; followed by 28 (α-*SMA*) or 33 (*desmin* and *TGF-β1*) cycles, consisting of 60 s of denaturation at 94°C, 60 s of annealing at 60°C (α-*SMA* and *TGF-β1*) or 60 s at 55°C (*desmin*), and 60 s of extension at 72°C; and a final extension of 5 min at 72°C. Each reaction was repeated three times to ensure consistent data.

The amplified products were analyzed by electrophoresis on 2% agarose gels containing ethidium bromide and

Table 1. Primers used for the semiquantitative polymerase chain reaction (RT-PCR) and the real-time quantitative PCR (qRT-PCR).

Gene	Forward primer 5′-3′	Reverse primer 5′-3′	Size (bp)
Desmin	CCA ACT GAG AGA AGA AGC AGA G	CTT ATT GGC TGC CTG AGT CAA G	259
α-SMA	GTT TGA GAC CTT CAA TGT CCC	CGA TCT CAC GCT CAG CAG TGA	334
TGF-β1	ATA CGC CTG AGT GGC TGT CT	TGG GAC TGA TCC CAT TGA TT	153
Cyclophilin	GGG AAG GTG AAA GAA GGC AT	GAG AGC AGA GAT TAC AGG GT	211
HPRT	CTC ATG GAC TGA TTA TGG ACA GGA C	GCA GGT CAG CAA AGA ACT TAT AGC C	123

visualized with an ultraviolet transilluminator (Gibco BRL, Life Technologies, USA). Gel images were captured with the Kodak Gel Logic 100 Imaging System (Kodak, USA). The density of the amplified bands was determined with the Kodak Molecular Imaging Software (version 4.0.5) and reported in arbitrary units (AU).

qRT-PCR

qRT-PCR was performed using the Rotor-Gene Q 5plex HRM thermal cycler (Qiagen, Germany). Each 15-μL reaction contained 100 ng cDNA, 0.3 μL gene-specific forward and reverse primers (10 μM), and 7.5 μL Platinum Sybr Green qRT-PCR SuperMix-UDG kit (Invitrogen). The cycling conditions were as follows: initial template denaturation for 5 min at 95°C, followed by 40 cycles of denaturation at 95°C for 20 s, annealing at 60°C for 30 s, and extension at 72°C for 30 s. Fluorescence detection was performed during each cycle at 72°C to identify the positive samples. Each sample was assessed in triplicate, and controls without template were included in parallel for each reaction. Amplification was followed by a melting curve analysis to check PCR product specificity. The fold changes in gene expression relative to the levels obtained in healthy rats, which were set equal to 1, were analyzed and calculated using the $2^{-\Delta\Delta ct}$ method (13).

Detection thresholds of RT-PCR and qRT-PCR

To compare the sensitivity and detection threshold of both methods, we measured α-actin levels in serial dilutions. A cDNA pool from all of the BO samples was serially diluted (1:10, 1:100, 1:1000, 1:10,000, 1:100,000) using the same reagents as previously described for each method.

Statistical analysis

Statistical analyses were performed using the SPSS software 18.0 for Windows (SPSS, USA). The Shapiro-Wilk test was used to determine whether groups of data had a Gaussian distribution. The significance of between-group differences was examined using one-way analysis of variance (ANOVA) and the Tukey multiple comparison *post hoc* test or a Kruskal-Wallis test and the Dunn *post hoc* test. P values <0.05 (two-tailed) were considered to be significant. The results are reported as the 25th and 75th percentiles, medians, and minimum and maximum values in box plots.

Results

Desmin, *α-SMA*, and *TGF-β1* expression in control, BO, and WBO parenchyma 7 days and 60 days after surgery are illustrated in box plots (Figure 2). The ordinate axis values represent the relative density of the RT-PCR bands and the values obtained by qRT-PCR. Semiquantitative RT-PCR analysis of the *desmin* gene showed no significant differences between the groups. However, the qRT-PCR evaluation of the same gene revealed an increase in *desmin* expression in the WBO parenchyma 7 days ($P=0.002$) and 60 days ($P=0.018$) after surgery compared with the control group.

The semiquantitative and quantitative analyses of *α-SMA* expression in the control, BO and WBO parenchyma 7 and 60 days after surgery are shown in Figure 3. Semiquantitative RT-PCR detected an increase in expression levels in the BO parenchyma 7 days after surgery ($P=0.004$). After 60 days, the same method detected an increase in *α-SMA* expression in both the BO ($P=0.008$) and WBO ($P=0.029$) parenchyma. Analysis by qRT-PCR confirmed these findings, showing an increase in expression level 7 days after surgery in the BO parenchyma ($P=0.003$) and 60 days after surgery in both the BO ($P=0.017$) and WBO ($P=0.023$) parenchyma.

The qRT-PCR analysis revealed increased expression of *TGF-β1* in the BO parenchyma 7 days after surgery compared with the control group ($P=0.015$). However, evaluation by RT-PCR detected no differences between the groups. No significant differences were observed by either method 60 days after surgery (Figure 4).

Evaluation of the detection threshold of each method indicated that RT-PCR was less sensitive at detecting small amounts of genetic material compared to qRT-PCR (Figure 5). Using serial dilutions of the cDNA, the semiquantitative method was only capable of detecting genetic material in dilutions with higher concentrations of cDNA (1:10 to 1:1000), whereas the qRT-PCR method allowed the visualization of real-time amplification in more dilute samples (1:10 to 1:100,000). Therefore, the high specificity of the qRT-PCR method was demonstrated even in samples with low concentrations of genetic material.

Discussion

The role of paracrine and endocrine mechanisms in

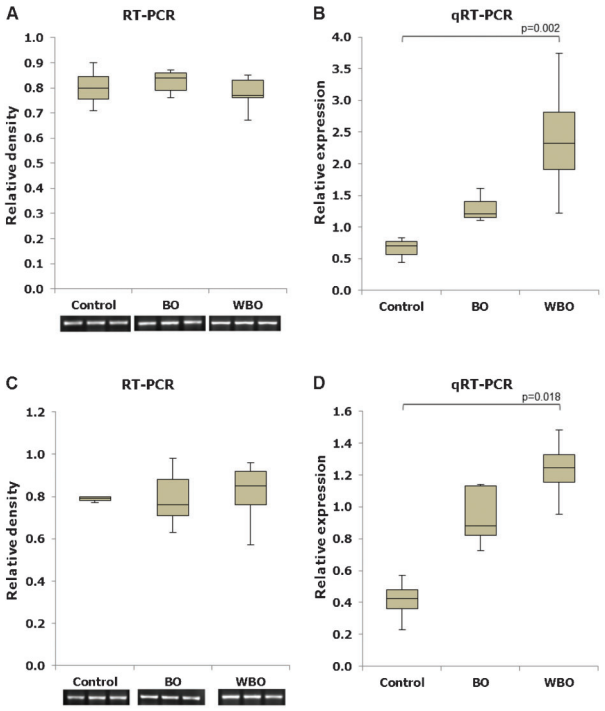

Figure 2. Gene expression profile of *desmin* from control rats, BO and WBO parenchymas. *A*, *C*, Semiquantitative analysis (RT-PCR) of the relative density at 7 days (*A*) and 60 days (*C*) after selective ligation of the bile duct. *B*, *D*, Quantitative analysis (qRT-PCR) at 7 days (*B*) and 60 days (*D*) after selective ligation of the bile duct. The gene expression values were obtained by relative quantification using the $2^{-\Delta\Delta ct}$ method. BO: biliary obstruction; WBO: without biliary obstruction. One-way ANOVA was used for the statistical analyses.

liver fibrosis progression has been proposed by many investigators (5-7). The evolution to cirrhosis, even after a successful Kasai portoenterostomy, and the fact that segmental biliary stenosis after liver transplantation may lead to cirrhosis of the whole organ, is most likely explained by paracrine/endocrine factors. In fact, in our model of selective biliary ligation, obstruction of the biliary ducts responsible for drainage of the median, left lateral, and caudate lobes was followed by biliary proliferation and portal fibrosis in the whole liver, including the unobstructed right lobe (1). In the present study, we evaluated the molecular events involved in the liver fibrogenic process in a model of selective biliary ligation using two methods of gene expression analysis (RT-PCR and qRT-PCR).

Comparison of the results obtained from each expression analysis method showed heterogeneity. These findings are of considerable interest in clinical and experimental research, as these methods are both commonly used, and can thus lead to different results between studies. The use of gene expression analysis to study experimental models of liver fibrosis is still infrequent, although these data may identify early pathophysiological changes involved in disease development (14,15). In our experimental model, the utilization of gene expression analysis techniques enabled the elucidation of the dynamic alterations in liver parenchyma driven by selective obstruction of the bile duct.

In the classical model of common bile duct ligation, activation and transdifferentiation of stellate cells into myofibroblasts are observed a few days after the obstruction of bile flow (9,16,17). Using the current model of selective bile duct ligation, qRT-PCR revealed an increase in *desmin* expression in the WBO parenchyma, whereas there were no differences in the BO parenchyma. These data support the hypothesis that the development of fibrosis occurs via endocrine or paracrine mechanisms (5-7). The process of transdifferentiation of cells into myofibroblasts is observed in the early stage of liver fibrogenesis. During activation and proliferation, hepatic stellate cells show a significant increase in the levels of *desmin* (15,16). Few studies have demonstrated a role for *desmin* in liver fibrogenesis, probably because of the increased levels of *desmin* in the initial phase of fibrogenesis (9,18,19). This hypothesis is supported by the results obtained in our animal model because *desmin* expression was unchanged in the obstructed parenchyma. This result is most likely related to the fact that the evolution of hepatic fibrogenesis was more intense in the BO parenchyma, assuming that the peak of *desmin* expression occurred before the 7th day of surgery, and that these hepatic stellate cells had most likely already differentiated into myofibroblasts 7 days after biliary obstruction.

The α-*SMA* expression levels in animals subjected to surgery also corroborate this hypothesis. Both molecular analysis methods showed an increase in the expression of α-*SMA* in the BO parenchyma 7 days after selective ligation, whereas the response in the WBO parenchyma was delayed, and the levels of α-*SMA* increased only 60 days after surgery. α-*SMA* is expressed by myofibroblasts, which are a heterogeneous population of highly pro-fibrogenic cells, and high levels indicate the progression of fibrosis with collagen deposition and a consequent alteration of parenchymal architecture (20,21). In experimental studies of fibrosis, this myofibroblast marker is highly expressed a few days after induction of fibrosis. In experimental models of common bile duct ligation and those induced by hepatotoxic drugs, application of a fibrogenic stimulus is followed within a few days by a rapid evolution and high levels of α-*SMA* (15,16).

The model of selective bile duct ligation demonstrated a progressive development of fibrosis, and similar to the classic experimental models, the presence of myofibroblasts in the first week of surgery in the BO parenchyma indicated a rapid evolution of fibrosis in the hepatic parenchyma. This observation was also supported by the gene expression profile of *TGF-β1*. The results obtained using qRT-PCR identified high levels of *TGF-β1* 7 days

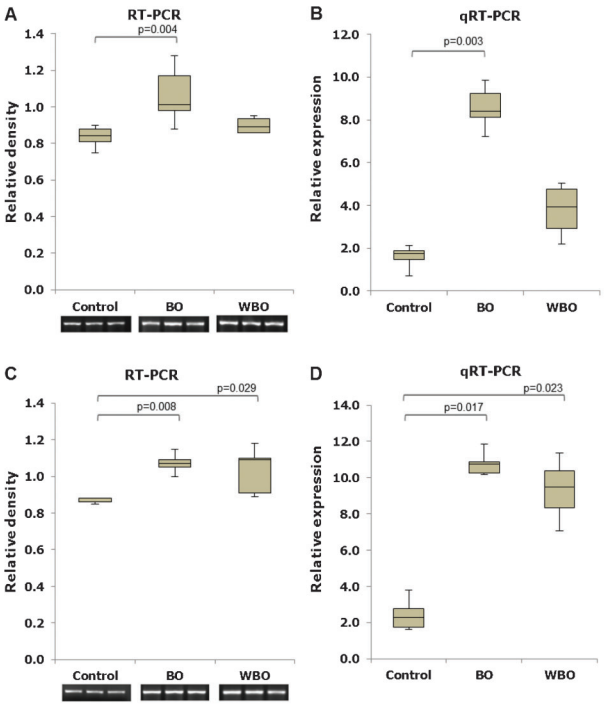

Figure 3. Gene expression profile of *alpha smooth muscle actin* (*α-SMA*) from control rats, BO and WBO parenchymas. *A*, *C*, Semiquantitative analysis (RT-PCR) of the relative density at 7 days (*A*) and 60 days (*C*) after selective ligation of the bile duct. *B*, *D*, Quantitative analysis (qRT-PCR) at 7 days (*B*) and 60 days (*D*) after selective ligation of the bile duct. The gene expression values were obtained by relative quantification using the $2^{-\Delta\Delta ct}$ method. One-way ANOVA was used for the comparisons of the semiquantitative method and the Kruskal-Wallis test was used for the qRT-PCR statistical analyses.

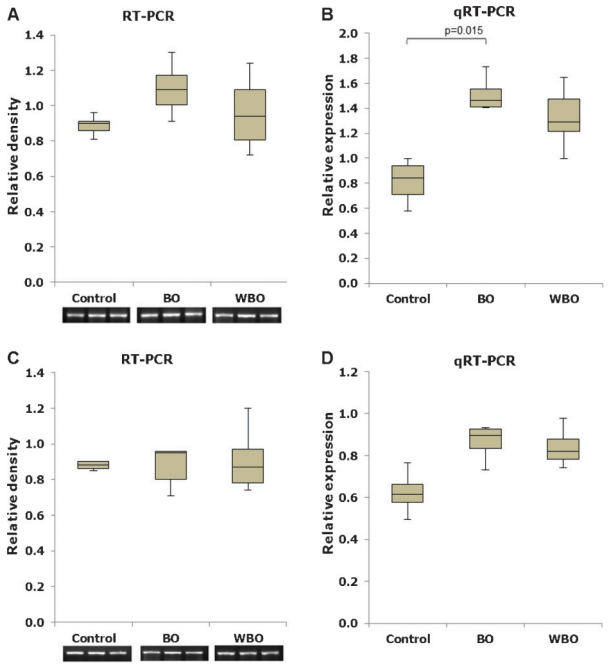

Figure 4. Gene expression profile of *TGF-β1* from control rats, BO and WBO parenchymas. *A*, *C*, Semiquantitative analysis (RT-PCR) of the relative density at 7 days (*A*) and 60 days (*C*) after selective ligation of the bile duct. *B*, *D*, Quantitative analysis (qRT-PCR) at 7 days (*B*) and 60 days (*D*) after selective ligation of the bile duct. The gene expression values were obtained by relative quantification using the $2^{-\Delta\Delta ct}$ method. One-way ANOVA was used for the statistical analyses.

after surgery in cholestatic liver parenchyma. *TGF-β1* is the main fibrogenic cytokine produced by myofibroblasts, and its expression is related to cell differentiation, particularly the stimulation of collagen synthesis (22-25). Furthermore, elevated levels of *TGF-β1* have been suggested to inhibit the proliferation of stellate cells, acting as an inducer of apoptosis and a negative feedback mechanism (26-28). Elevated levels of *TGF-β1* suggest that the responses to fibrogenic mechanisms were more intense in the liver parenchyma with biliary obstruction, in which the presence of this cytokine is closely related to the deposition of type I collagen by myofibroblasts. After 60 days, stellate cell proliferation was suppressed by *TGF-β1*, and myofibroblast cytokine production also returned to control levels.

In our investigation, the semiquantitative results from RT-PCR were unable to describe the molecular mechanisms involved in the modulation of hepatic fibrogenesis. We found that the observed differences for *α-SMA* using the semiquantitative method were similar to the results obtained using qRT-PCR. When *TGF-β1* levels were evaluated using the two different methods, the semiquantitative method detected an increased, but not significantly different, expression level in the BO parenchyma ($P = 0.09$). These findings were further refined using qRT-PCR, which showed that the BO liver parenchyma was significantly different from the control group ($P = 0.015$). As previously stated, desmin is an acute-phase protein that is expressed at high levels during the activation and proliferation of hepatic stellate cells (15,16). In our study, we examined the process of fibrogenesis in its initial phase. It was not possible to identify differences between the groups using RT-PCR. However, qRT-PCR detected changes in *desmin* expression levels in liver parenchyma with biliary drainage normal. The discrepancies between the different methods can be explained by the higher sensitivity of qRT-PCR in detecting small changes in transcript level (29). In fact, in evaluating the cDNA detection limit using RT-PCR and qRT-PCR, Dagher et al. (30) demonstrated that the real-time quantitative method is 10-fold more sensitive than the semiquantitative method for detection of low sample concentrations.

To compare the effectiveness of both methods in distinguishing small amounts of genetic material, we performed serial dilutions of cDNA and qualitatively

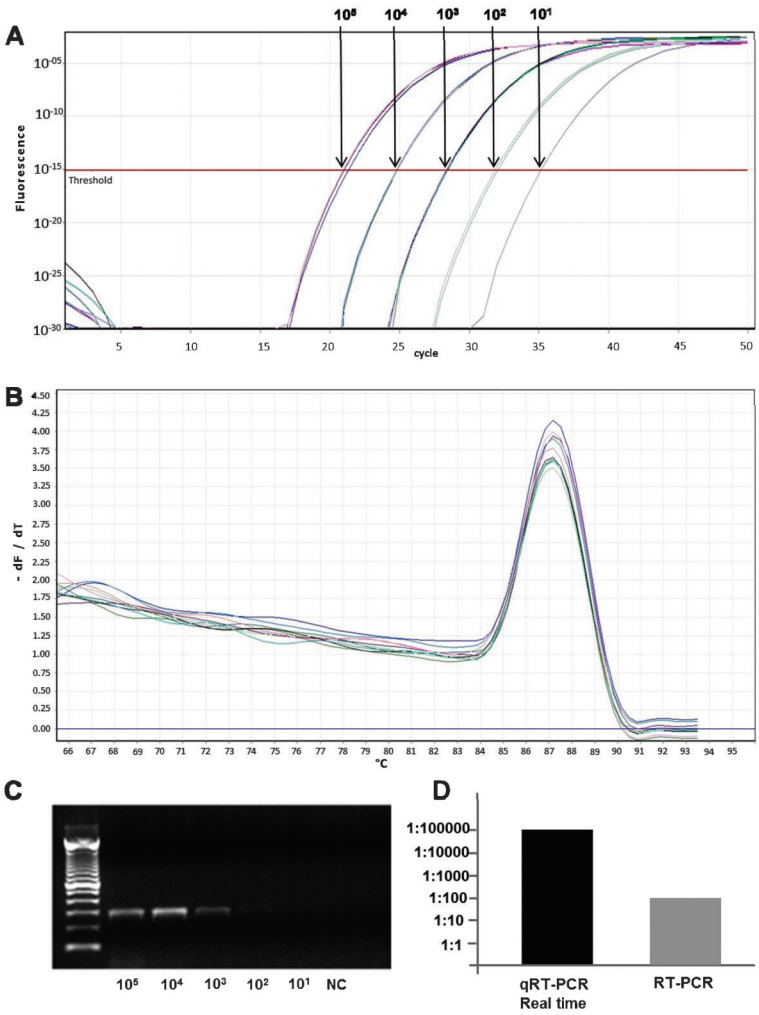

Figure 5. Comparison of the detection limit of alpha smooth muscle actin (α-SMA) cDNA using semiquantitative PCR (RT-PCR) and quantitative real-time PCR (qRT-PCR). cDNA from all of the samples was 10-fold serially diluted. *A*, Amplification curve generated by plotting SYBR Green I fluorescence data (y-axis) collected at each cycle (x-axis) during the extension phase of the PCR. cDNA copy number per sample: (10^5, 10^4, 10^3, 10^2, 10^1). *B*, Melting curve analysis obtained by plotting the negative derivative of fluorescence over temperature (-dF/dT) (y-axis) *vs* temperature in degrees Celsius (°C) (x-axis) showing the specificity of the PCR assay for samples with a small amount of genetic material. *C*, Samples amplified using RT-PCR and analyzed with gel electrophoresis. Note that only three dilutions of cDNA were detected (10^5, 10^4, 10^3). *D*, Graphical representation of the detection efficiency of the diluted samples by the methods of RT-PCR and qRT-PCR. NC: negative control.

compared the ability of the methods to amplify cDNA in each dilution. Using this experimental design, the detection limit for the semiquantitative method was shown to be lower, and the amplified product was not detectable in samples diluted more than 1:1,000. In contrast, qRT-PCR showed higher levels of sensitivity and was capable of detecting cDNA in samples containing smaller amounts than the other method, including in dilutions of 1:100,000, as well as demonstrating a high specificity as assessed by the melting curve.

These findings can also be compared with previous results of the gene analyses in our experimental model. From the scale of the graphs of the levels of alpha-actin gene expression, it is possible to see that the results obtained from the qRT-PCR showed higher values that are easy to distinguish from one another. In the semiquantitative method, the scale of gene expression values was smaller, although statistically significant. In addition, no significant differences in *desmin* and *TGF-β1* expression were observed in BO and WBO parenchymas using the semiquantitative method, but in graphical scale qRT-PCR low values were revealed.

By examining the results obtained using both gene expression analysis methods, we elucidated the molecular mechanisms involved in liver fibrogenesis in an experimental model of selective bile duct ligation. In summary, we demonstrated an increase in *desmin* expression at the beginning of the fibrogenic process that is involved in the proliferation of hepatic stellate cells. The liver parenchyma subjected to bile duct ligation showed a more intense fibrogenic response, with cells differentiating into myofibroblasts a few days after surgery, as identified by the increase in *α-SMA* expression. As fibrogenesis in the liver parenchyma with an obstruction of bile flow occurs, an endocrine or paracrine mechanism promotes activation of the fibrogenic process in the WBO-adjacent hepatic parenchyma. These findings were confirmed by the expression of *desmin* early in the process and the delayed expression of *α-SMA*, demonstrating a slower progression of hepatic fibrogenesis in the WBO parenchyma. The increased levels of *TGF-β1* expression were correlated

with collagen deposition in the cholestatic liver parenchyma (BO). During the process of hepatic fibrogenesis, the role of *TGF-β1* is complex because it is related to cell differentiation, collagen deposition, and inhibition of hepatic stellate cell proliferation (24,25,28,31). Our results agree with the theoretical basis found in the literature, because the inhibition of stellate cell proliferation by *TGF-β1* was related to low levels of *desmin* expression in the liver parenchyma with cholestasis, even early in the fibrogenic process.

In conclusion, our data support the hypothesis that the fibrogenic stimulus from a hepatic segment with biliary obstruction causes subsequent development of fibrosis in the adjacent parenchyma. Using gene expression analysis, we established the molecular dynamic changes involved in the fibrogenic process in this experimental model, allowing its inclusion in studies of alterations of segmental cholestasis such as intrahepatic biliary stenosis and biliary atresia.

References

1. Tannuri AC, Coelho MC, de Oliveira Goncalves J, Santos MM, Ferraz da Silva LF, Bendit I, et al. Effects of selective bile duct ligation on liver parenchyma in young animals: histologic and molecular evaluations. *J Pediatr Surg* 2012; 47: 513-522, doi: 10.1016/j.jpedsurg.2011.10.009.
2. Tannuri U, Velhote MC, Santos MM, Gibelli NE, Ayoub AA, Maksoud-Filho JG, et al. Pediatric liver transplantation: fourteen years of experience at the children institute in Sao Paulo, Brazil. *Transplant Proc* 2004; 36: 941-942, doi: 10.1016/j.transproceed.2004.03.101.
3. Karakayali F, Kirnap M, Akdur A, Tutar N, Boyvat F, Moray G, et al. Biliary complications after pediatric liver transplantation. *Transplant Proc* 2013; 45: 3524-3527, doi: 10.1016/j.transproceed.2013.09.012.
4. Wadhawan M, Kumar A, Gupta S, Goyal N, Shandil R, Taneja S, et al. Post-transplant biliary complications: an analysis from a predominantly living donor liver transplant center. *J Gastroenterol Hepatol* 2013; 28: 1056-1060, doi: 10.1111/jgh.12169.
5. Glaser S, DeMorrow S, Francis H, Ueno Y, Gaudio E, Vaculin S, et al. Progesterone stimulates the proliferation of female and male cholangiocytes via autocrine/paracrine mechanisms. *Am J Physiol Gastrointest Liver Physiol* 2008; 295: G124-G136, doi: 10.1152/ajpgi.00536.2007.
6. Marzioni M, Glaser S, Francis H, Marucci L, Benedetti A, Alvaro D, et al. Autocrine/paracrine regulation of the growth of the biliary tree by the neuroendocrine hormone serotonin. *Gastroenterology* 2005; 128: 121-137, doi: 10.1053/j.gastro.2004.10.002.
7. Gaudio E, Barbaro B, Alvaro D, Glaser S, Francis H, Ueno Y, et al. Vascular endothelial growth factor stimulates rat cholangiocyte proliferation via an autocrine mechanism. *Gastroenterology* 2006; 130: 1270-1282, doi: 10.1053/j.gastro.2005.12.034.
8. Novo E, di Bonzo LV, Cannito S, Colombatto S, Parola M. Hepatic myofibroblasts: a heterogeneous population of multifunctional cells in liver fibrogenesis. *Int J Biochem Cell Biol* 2009; 41: 2089-2093, doi: 10.1016/j.biocel.2009.03.010.
9. Ballardini G, Fallani M, Biagini G, Bianchi FB, Pisi E. Desmin and actin in the identification of Ito cells and in monitoring their evolution to myofibroblasts in experimental liver fibrosis. *Virchows Arch B Cell Pathol Incl Mol Pathol* 1988; 56: 45-49, doi: 10.1007/BF02890000.
10. Henderson NC, Sheppard D. Integrin-mediated regulation of TGFbeta in fibrosis. *Biochim Biophys Acta* 2013; 1832: 891-896, doi: 10.1016/j.bbadis.2012.10.005.
11. Rosenbloom J, Mendoza FA, Jimenez SA. Strategies for anti-fibrotic therapies. *Biochim Biophys Acta* 2013; 1832: 1088-1103, doi: 10.1016/j.bbadis.2012.12.007.
12. COBEA (Colégio Brasileiro de Experimentação Animal). Ethic Commission for animal experimentation. http://www.cobea.org.br.
13. Livak KJ, Schmittgen TD. Analysis of relative gene expression data using real-time quantitative PCR and the 2(-Delta Delta C(T)) Method. *Methods* 2001; 25: 402-408, doi: 10.1006/meth.2001.1262.
14. Chobert MN, Couchie D, Fourcot A, Zafrani ES, Laperche Y, Mavier P, et al. Liver precursor cells increase hepatic fibrosis induced by chronic carbon tetrachloride intoxication in rats. *Lab Invest* 2012; 92: 135-150, doi: 10.1038/labinvest.2011.143.
15. Golbar HM, Izawa T, Yano R, Ichikawa C, Sawamoto O, Kuwamura M, et al. Immunohistochemical characterization of macrophages and myofibroblasts in alpha-Naphthylisothiocyanate (ANIT) - induced bile duct injury and subsequent fibrogenesis in rats. *Toxicol Pathol* 2011; 39: 795-808, doi: 10.1177/0192623311413790.
16. Gibelli NE, Tannuri U, Mello ES. Immunohistochemical studies of stellate cells in experimental cholestasis in newborn and adult rats. *Clinics* 2008; 63: 689-694, doi: 10.1590/S1807-59322008000500019.
17. Iredale JP, Thompson A, Henderson NC. Extracellular matrix degradation in liver fibrosis: Biochemistry and regulation. *Biochim Biophys Acta* 2013; 1832: 876-883, doi: 10.1016/j.bbadis.2012.11.002.
18. Ballardini G, Groff P, Badiali de Giorgi L, Schuppan D, Bianchi FB. Ito cell heterogeneity: desmin-negative Ito cells in normal rat liver. *Hepatology* 1994; 19: 440-446, doi: 10.1002/hep.1840190224.
19. Takase S, Leo MA, Nouchi T, Lieber CS. Desmin distinguishes cultured fat-storing cells from myofibroblasts, smooth muscle cells and fibroblasts in the rat. *J Hepatol* 1988; 6: 267-276, doi: 10.1016/S0168-8278(88)80042-4.
20. Gressner AM. Transdifferentiation of hepatic stellate cells (Ito cells) to myofibroblasts: a key event in hepatic fibrogenesis. *Kidney Int Suppl* 1996; 54: S39-S45.
21. Lee UE, Friedman SL. Mechanisms of hepatic fibrogenesis. *Best Pract Res Clin Gastroenterol* 2011; 25: 195-206, doi: 10.1016/j.bpg.2011.02.005.
22. Kaimori A, Potter J, Kaimori JY, Wang C, Mezey E, Koteish A. Transforming growth factor-beta1 induces an epithelial-to-mesenchymal transition state in mouse hepatocytes *in vitro*. *J Biol Chem* 2007; 282: 22089-22101, doi: 10.1074/jbc.M700998200.
23. Lewindon PJ, Pereira TN, Hoskins AC, Bridle KR,

Williamson RM, Shepherd RW, et al. The role of hepatic stellate cells and transforming growth factor-beta(1) in cystic fibrosis liver disease. *Am J Pathol* 2002; 160: 1705-1715, doi: 10.1016/S0002-9440(10)61117-0.
24. Lijnen P, Petrov V. Transforming growth factor-beta 1-induced collagen production in cultures of cardiac fibroblasts is the result of the appearance of myofibroblasts. *Methods Find Exp Clin Pharmacol* 2002; 24: 333-344, doi: 10.1358/mf.2002.24.6.693065.
25. Meindl-Beinker NM, Dooley S. Transforming growth factor-beta and hepatocyte transdifferentiation in liver fibrogenesis. *J Gastroenterol Hepatol* 2008; 23 (Suppl 1): S122-S127, doi: 10.1111/j.1440-1746.2007.05297.x.
26. Dooley S, Delvoux B, Lahme B, Mangasser-Stephan K, Gressner AM. Modulation of transforming growth factor beta response and signaling during transdifferentiation of rat hepatic stellate cells to myofibroblasts. *Hepatology* 2000; 31: 1094-1106, doi: 10.1053/he.2000.6126.
27. Jakowlew SB, Mead JE, Danielpour D, Wu J, Roberts AB, Fausto N. Transforming growth factor-beta (TGF-beta) isoforms in rat liver regeneration: messenger RNA expression and activation of latent TGF-beta. *Cell Regul* 1991; 2: 535-548.
28. Schrum LW, Bird MA, Salcher O, Burchardt ER, Grisham JW, Brenner DA, et al. Autocrine expression of activated transforming growth factor-beta(1) induces apoptosis in normal rat liver. *Am J Physiol Gastrointest Liver Physiol* 2001; 280: G139-G148.
29. Schmittgen TD, Zakrajsek BA, Mills AG, Gorn V, Singer MJ, Reed MW. Quantitative reverse transcription-polymerase chain reaction to study mRNA decay: comparison of endpoint and real-time methods. *Anal Biochem* 2000; 285: 194-204, doi: 10.1006/abio.2000.4753.
30. Dagher H, Donninger H, Hutchinson P, Ghildyal R, Bardin P. Rhinovirus detection: comparison of real-time and conventional PCR. *J Virol Methods* 2004; 117: 113-121, doi: 10.1016/j.jviromet.2004.01.003.
31. Bachem MG, Meyer D, Melchior R, Sell KM, Gressner AM. Activation of rat liver perisinusoidal lipocytes by transforming growth factors derived from myofibroblastlike cells. A potential mechanism of self perpetuation in liver fibrogenesis. *J Clin Invest* 1992; 89: 19-27, doi: 10.1172/JCI115561.